

Granular Ball Guided Stable Latent Domain Discovery for Domain-General Crowd Counting

Fan Chen¹, Shuyin Xia*¹, Senior Member, IEEE, Yi Wang, Xinbo Gao¹, Fellow, IEEE

Abstract—Single-source domain generalization for crowd counting remains highly challenging because a single labeled source domain often contains heterogeneous latent domains, while test data may exhibit severe distribution shifts. A fundamental difficulty lies in stable latent domain discovery: directly performing flat clustering on evolving sample-level latent features is easily affected by feature noise, outliers, and representation drift, leading to unreliable pseudo-domain assignments and weakened domain-structured learning. To address this issue, we propose a granular ball guided stable latent domain discovery framework for domain-general crowd counting. Specifically, the proposed method first organizes samples into compact local granular balls and then clusters granular ball centers as representatives to obtain pseudo-domains, transforming direct sample-level clustering into a hierarchical representative-based clustering process. This design yields more stable and semantically consistent pseudo-domain assignments. Built upon the discovered latent domains, we further develop a two-branch learning framework that enhances transferable semantic representations via semantic codebook re-encoding while modeling domain-specific appearance variations through a style branch, thereby reducing semantic-style entanglement and improving generalization under domain shifts. Extensive experiments on ShanghaiTech A/B, UCF_QNRF, and NWPU-Crowd under a strict no-adaptation protocol demonstrate that the proposed method consistently outperforms strong baselines, especially under large domain gaps.

Index Terms—Crowd counting, domain generalization, single-source domain generalization, stable latent domain discovery, granular ball, disentangled representation learning.

I. INTRODUCTION

Crowd counting aims to estimate the number of people in an image, typically by predicting a density map whose integral yields the final count [1]–[8]. It plays a critical role in public safety monitoring, large-scale event management, and intelligent transportation. Recent advances have been largely driven by deep neural networks. However, most counting models rely on the assumption that the deployment data distribution matches the training distribution, and their performance can drop drastically when deployed to data distributions different from those seen during training [1], [2], [9]. In real-world applications, crowd images collected across different cities, cameras, and time periods often exhibit substantial domain shifts, including changes in density levels, viewpoints, scene layouts, illumination, and background clutter [10], [11]. Such

This work was supported by Chongqing Key Laboratory of Computational Intelligence, Key Laboratory of Cyberspace Big Data Intelligent Security, Ministry of Education, Sichuan-Chongqing Co-construction Key Laboratory of Digital Economy Intelligence, and Key Laboratory of Big Data Intelligent Computing, Chongqing University of Posts and Telecommunications.

*Corresponding author: Shuyin Xia (xiasy@cqupt.edu.cn), Chongqing University of Posts and Telecommunications, China.

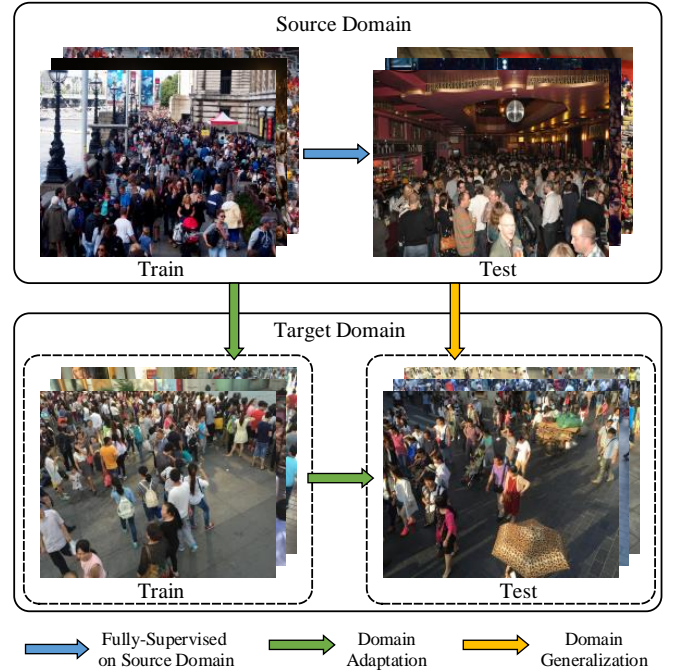


Fig. 1. Motivation and settings under domain shift. Fully-supervised assumes matched source train/test distributions. Domain adaptation aligns with target-domain training data. Domain generalization trains on labeled source only and directly tests on unseen targets without adaptation.

shifts are particularly challenging for density regression, as accurate counting relies on both semantic cues and fine-grained texture and scale patterns [2]–[4]. Meanwhile, annotating dense point labels or density maps for every new environment is expensive and sometimes infeasible [12], [13]. A common way to address domain shift is domain adaptation, which leverages unlabeled or sparsely labeled target data to reduce distribution gaps [14], [15]. However, target data may be unavailable due to privacy constraints, limited access, or fast-changing deployment environments. This motivates domain generalization (DG): learning a counting model from a labeled source domain only, while generalizing to arbitrary unseen target domains without any further adaptation [9], [16], [17].

As illustrated in Fig. 1, existing counting pipelines under distribution shift can be roughly categorized into three settings. Fully-supervised methods assume that training and test images come from the same source domain, and thus performance deteriorates when the test distribution shifts. Domain adaptation alleviates this issue by exploiting unlabeled (or sparsely labeled) target-domain training data to align distributions

before testing, but it explicitly requires access to target data during training. In contrast, domain generalization targets a more practical deployment scenario: the model is trained only on the labeled source domain and is expected to generalize directly to arbitrary unseen target domains at test time, without any target-domain data or further adaptation.

A key challenge of single-source DG is that a “source domain” is rarely homogeneous. Instead, it usually contains multiple latent domains induced by diverse scenes, imaging conditions, and crowd patterns. Therefore, domain-general crowd counting is not only a problem of learning domain-invariant representations, but also a problem of reliably discovering latent domain structure hidden within the source set. Recent DG approaches attempt to partition the source data into pseudo-domains and exploit them to enhance robustness under domain shifts [18], [19]. Some recent works further leverage predictive uncertainty to guide style diversification for improving generalization [19]–[22]. However, a fundamental issue remains under-explored: stable latent domain discovery in an evolving feature space. Existing pseudo-domain discovery methods commonly rely on sample-level flat clustering over learned features, which is easily affected by noisy samples, outliers, and representation drift during training, resulting in unstable pseudo-domain assignments [18]. Moreover, even when pseudo-domains are available, it is still non-trivial to learn counting representations that preserve counting-relevant semantics while preventing domain-specific appearance factors from leaking into the shared representation [18], [19].

Granular Ball Computing (GBC) provides a promising perspective for addressing this challenge. As a lightweight paradigm for structural multi-granularity modeling, GBC organizes samples into compact granular balls that summarize local structure with ball-level representatives, and progressively refines the partition from coarse to fine [23]–[26]. This property is particularly appealing for latent domain discovery in single-source DG crowd counting. Compared with directly clustering individual samples, granular ball partitioning first aggregates locally consistent samples into compact structured groups and then uses granular ball centers as stable representatives for higher-level pseudo-domain grouping, thereby reducing sensitivity to noisy features and transient representation drift. In this way, latent domain discovery can be transformed from unstable sample-level flat clustering into a more robust hierarchical representative-based clustering process. Meanwhile, recent GBC studies have demonstrated its effectiveness in visual understanding and representation modeling, suggesting that granular ball structures can serve as efficient and interpretable units for adaptive multi-granularity computation [27]–[29].

Motivated by the above observations, we propose Granular Ball Guided Stable Latent Domain Discovery for domain-general crowd counting. Our key idea is to model the latent domain structure of a single source dataset from two complementary perspectives: stable structure discovery and structure-aware representation learning. First, we introduce a granular ball guided latent domain discovery strategy in a domain-sensitive feature space. Instead of directly clustering individual samples, we recursively partition the feature set into compact granular balls and then cluster granular ball centers as ball-

level representatives to obtain pseudo-domains. This coarse-to-fine and set-to-representative procedure transforms unstable sample-level flat clustering into a more robust hierarchical representative-based clustering process, thereby improving the stability of pseudo-domain assignments and enabling online refinement during training. Second, based on the discovered latent domains, we build a two-branch learning scheme on top of a shared multi-scale backbone. The semantic branch employs a learnable memory bank to re-encode semantic features into a compact and stable basis for density estimation, while the style branch captures domain-related appearance variations and provides regularization signals. By enforcing intra-domain style compactness and semantic–style orthogonality, the proposed framework reduces domain leakage and facilitates disentangled counting representation learning, leading to improved robustness under domain shifts [18], [19].

We evaluate our approach on standard DG crowd counting benchmarks and demonstrate consistent improvements over strong baselines across multiple cross-domain transfer settings. In particular, our method yields clear gains on challenging transfers such as SHB→QNRF, highlighting the effectiveness of granular ball guided stable latent domain discovery and semantic memory re-encoding under large domain gaps.

Our main contributions are summarized as follows:

- We identify stable latent domain discovery as a key bottleneck in single-source domain-general crowd counting, and show that existing sample-level flat clustering strategies are vulnerable to noisy features, outliers, and representation drift in evolving latent spaces.
- We propose a granular ball guided stable latent domain discovery method that first partitions samples into compact granular balls and then clusters granular ball centers as representatives, thereby transforming direct sample-level clustering into a hierarchical representative-based clustering process and yielding more stable pseudo-domain assignments.
- We develop a structure-aware counting framework built upon the discovered latent domains, with semantic memory re-encoding and style regularization, which enhances domain-invariant semantic learning while suppressing domain-specific appearance leakage, and thus improves generalization to unseen domains.

The remainder of this paper is organized as follows. Section III presents the proposed method. Section IV reports experimental results and ablation studies. Finally, we conclude the paper in Section V.

II. RELATED WORK

A. Crowd Counting

Most modern crowd counting methods formulate counting as density regression, where a network predicts a density map and the integral over the map yields the final count. Early deep approaches addressed large scale variation by using multi-branch or multi-column architectures, such as MCNN [1]. Subsequent works improved representation learning for highly congested scenes and complex backgrounds, including CSR-Net with dilated convolutions [2], scale aggregation designs

for multi-scale robustness [4], and context-aware counting that adaptively selects contextual cues across locations [5]. More recently, transformer-based models have been explored to enhance global modeling and cross-view interaction, such as multi-view counting transformers [30], and discriminative feature learning has also been studied to improve counting robustness under diverse scenes [31].

Beyond network architecture, supervision design and loss functions are extensively investigated to reduce annotation noise and improve generalization. Composition loss jointly considers counting, density estimation, and localization objectives [10], while Bayesian loss provides a probabilistic formulation for point-supervised counting without relying on imperfect pixel-wise density targets [6]. Distribution matching further mitigates the bias introduced by Gaussian-smoothed density labels by aligning predicted and target density distributions [3]. Frequency-domain objectives have also been introduced for crowd analysis to better capture distributional characteristics [32]. In addition, large-scale benchmarks such as NWPU-Crowd facilitate evaluation under diverse scenes and density levels and have become standard testbeds for crowd counting [11].

Recent research also emphasizes data efficiency, modality extension, and deployability. Semi-supervised learning has been actively explored to alleviate annotation cost, including strong data/model boosting strategies [33] and density distribution modeling for reliable pixel-level supervision [34]. Multi-modal crowd counting has emerged to leverage complementary cues, e.g., using a broker modality to bridge heterogeneous modalities [35], and further improvements can be obtained by plug-and-play enhancement strategies [36]. Generative modeling has also been introduced to produce diverse plausible density hypotheses, such as diffusion-based crowd density estimation [37]. Meanwhile, efficient and deployable counting has received increasing attention, including lightweight encoder-decoder designs [7] and knowledge distillation based counting frameworks that transfer dense prediction knowledge from stronger teachers to compact students [8].

B. Domain Generalization

Crowd counting models trained on a single dataset often exhibit severe performance degradation when deployed to unseen environments, due to substantial distribution shifts in crowd density, viewpoint, illumination, and background clutter [10], [11]. To improve robustness under domain shifts, two closely related research lines are domain adaptation and domain generalization. Domain adaptation assumes access to unlabeled or sparsely labeled target-domain data and aims to reduce the source-target discrepancy through distribution alignment. Representative techniques include adversarial feature alignment and correlation alignment [14], [15]. In crowd counting, adaptation has been explored through cross-domain transfer mechanisms such as density reconstruction and unlabeled scene adaptation [12], [13], as well as domain-agnostic alignment based on optimal transport [38]. Other works leverage unlabeled target data through knowledge diffusion for unsupervised cross-domain counting [39]. Although effective

when target data is available, adaptation may be impractical in real deployments due to privacy concerns, limited access, or fast-changing environments.

Domain generalization (DG), in contrast, learns from labeled source data only and requires the trained model to generalize to unseen target domains without any adaptation. General DG methods typically pursue domain-invariant representations through data or style perturbation, regularization, or normalization-based strategies [9], [16], [17]. Recent studies also explore more structured learning paradigms, such as learning from multiple experts [40], or combining normalization layers and regularization for robust generalization in federated settings [41]. For crowd counting, recent DG approaches have paid increasing attention to the single-source setting by uncovering latent sub-domains within the source set and exploiting pseudo-domain supervision to facilitate generalization [18], [42]. In addition, style-based diversification has been shown beneficial for robustness, and predictive uncertainty can further guide style augmentation under distribution shifts [19]–[22].

Despite this progress, existing single-source DG crowd counting methods still leave two issues insufficiently addressed. First, pseudo-domain discovery is commonly performed via sample-level flat clustering on evolving latent features, which is vulnerable to feature noise, outliers, and representation drift, and may therefore lead to unstable pseudo-domain assignments [18], [42]. Second, even when pseudo-domains are available, it remains challenging to learn counting representations that preserve counting-relevant semantics while suppressing domain-specific appearance factors, especially under large domain gaps [18], [19]. These observations suggest the need for a more robust structural modeling perspective for single-source DG crowd counting, which motivates the method presented next.

C. Granular Ball Computing

Psychophysical evidence suggests that human visual perception tends to capture global structure before local details [43], which motivates multi-granularity representations for complex visual understanding. In granular computing, Wang et al. [23] advocated multi-granular cognitive computing, and Xia et al. [24] further introduced Granular Ball Computing (GBC) as a lightweight paradigm for adaptive multi-granularity modeling. GBC represents the sample space by a set of granular balls with varying sizes, where each ball summarizes local data distribution by a center and an adaptive radius, and a hierarchical partition can be obtained by recursively generating and refining balls from coarse to fine [24], [44].

A key advantage of GBC lies in its efficiency, robustness, and interpretability under noisy and heterogeneous data. To this end, a series of granular ball generation and learning algorithms have been developed, including Ball k - k -means for fast adaptive clustering [45], efficient and adaptive ball generation for classification [44], and multi-granularity neighbor relationships that benefit KNN-style learning and clustering [46]. Recent studies have also extended GBC to broader learning settings, such as uncertainty-aware or cognitively motivated representation learning in reinforcement learning [47],

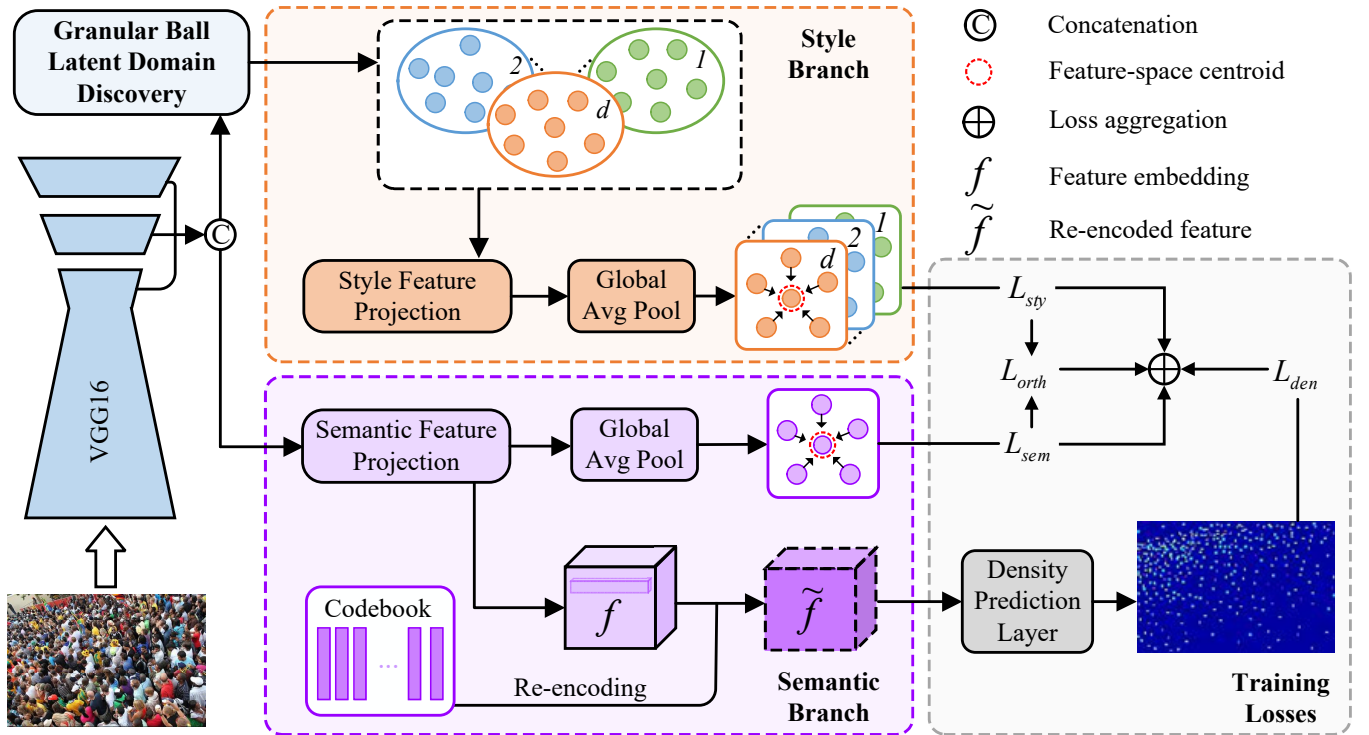


Fig. 2. Overall framework of the proposed method, consisting of semantic codebook re-encoding, style-branch regularization, and granular ball guided stable latent domain discovery for robust density regression.

granular ball based support vector machines [28], and scalable learning on large graphs via supervised granular ball based graph coarsening [48]. Moreover, GBC has shown promise in vision-oriented representation modeling, e.g., adaptive multi-granularity graph representations of images [29].

These properties make GBC a promising tool for modeling latent structure in single-source domain generalization. Compared with sample-level flat clustering, granular ball modeling aggregates multiple samples into compact local sets and provides ball-level representatives, which are potentially less sensitive to noisy features, outliers, and representation drift during training. In particular, granular ball centers offer representative prototypes for higher-level grouping, making GBC well aligned with the requirement of stable latent domain discovery in evolving feature spaces. Therefore, GBC provides a natural structural perspective for pseudo-domain partitioning and representation learning in domain-general crowd counting.

III. METHOD

Granular Ball Computing (GBC) models data by a set of compact local structural units, where each granular ball summarizes a subset of samples using a representative center together with associated structural attributes. By recursively splitting and refining balls from coarse to fine, GBC provides a hierarchical multi-granularity partition of the underlying feature space. In this work, we instantiate this idea in latent domain discovery, where granular balls serve as stable local structural units for grouping evolving sample representations. Formally, given a dataset $X = \{x_1, x_2, \dots, x_n\}$, we construct a granular ball set $GB = \{GB_1, GB_2, \dots, GB_m\}$ on X .

Each ball is defined as $GB_i = (X_i, c_i, \vec{\theta}_i)$, where $X_i \subset X$ denotes the covered subset, c_i is the ball center, and $\vec{\theta}_i$ includes other structural attributes beyond the standard spherical radius. Under this definition, the general GBC model can be written as:

$$\begin{aligned} f(X, \vec{\alpha}) &\longrightarrow g(GB, \vec{\beta}) \\ \min_{c_i, \vec{\theta}_i, \vec{\beta}, m} &\mathcal{J}(-Cov(GB), -Comp(GB)) + m \\ \text{s.t. } &quality(GB_i) \geq \phi(X), \quad i = 1, 2, \dots, m \\ &C(GB, X) \geq 0, \end{aligned} \quad (1)$$

where $f(X, \vec{\alpha})$ denotes a learning model on samples with parameters $\vec{\alpha}$, and $g(GB, \vec{\beta})$ denotes a ball-based model with parameters $\vec{\beta}$. The objective $\mathcal{J}(-Cov(GB), -Comp(GB))$ jointly considers coverage and compactness, while m regularizes the number of balls. The constraint $quality(GB_i) \geq \phi(X)$ determines whether a ball is acceptable or should be further split, and $C(GB, X)$ encodes structural relations among balls and samples. Overall, Eq. (1) reflects a transition from point-wise learning to multi-granularity ball-based computation.

As illustrated in Fig. 2, the proposed method learns robust counting representations by explicitly modeling the latent domain structure hidden in a single source dataset. Given an input image, we employ a VGG16-based encoder-decoder backbone to extract multi-level features, where three feature maps from different scales are upsampled to the same resolution and concatenated to form a unified representation F . Based on F , our method follows a two-branch design to separate semantic and style factors. The semantic branch focuses on domain-invariant

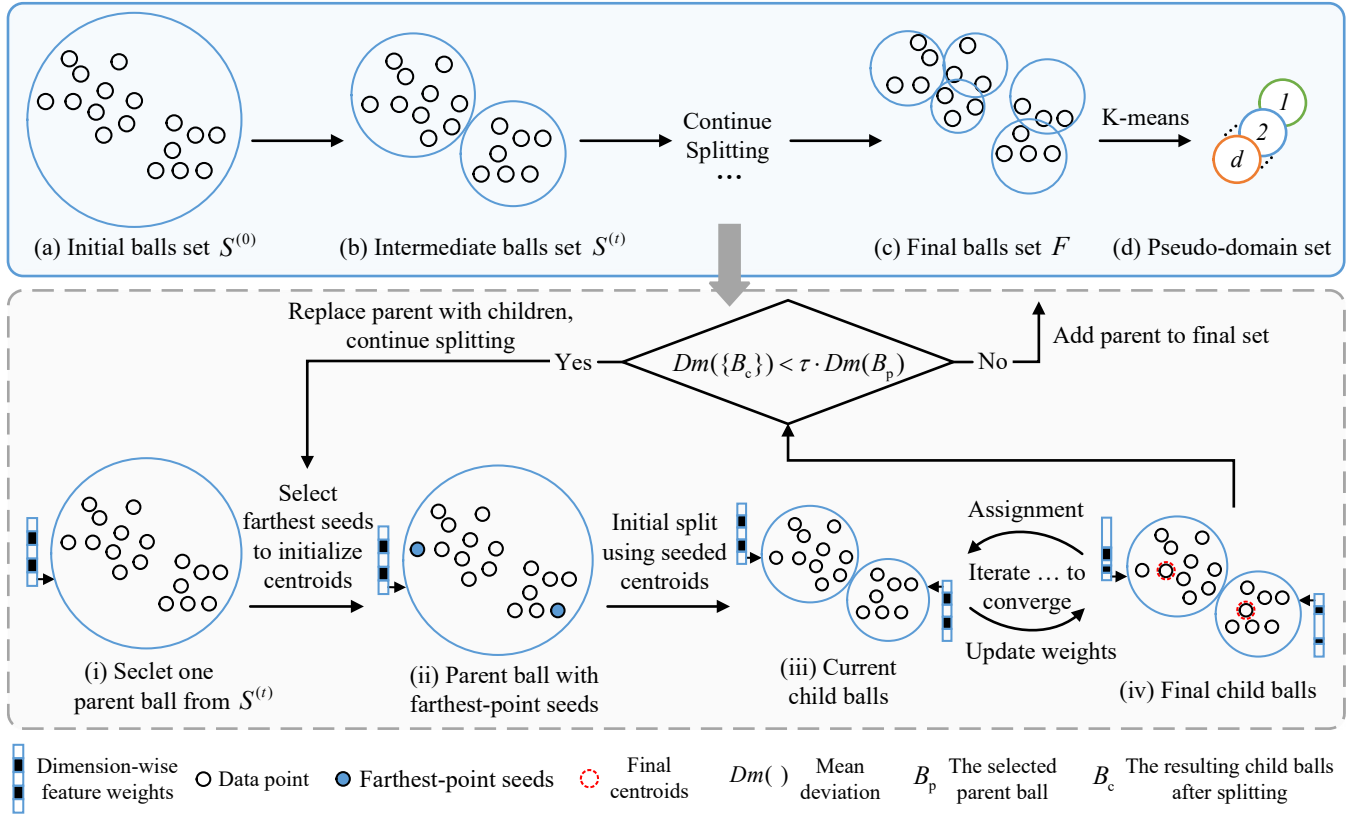


Fig. 3. Hierarchical division and merging of a weighted granular ball set (WGBS) for pseudo-domain discovery. Starting from the initial balls set $S^{(0)}$, we iteratively select a parent ball $B_p \in S^{(t)}$ and split it into two child balls via weighted 2-means (initialized by farthest-point seeding and iterated to convergence with weight updates). The split is accepted if the child compactness decreases, i.e., $Dm(\{B_c\}) < \tau \cdot Dm(B_p)$; otherwise, B_p is added to the final balls set F . After no further split is accepted, we obtain the final balls set F and run K -means on granular ball centers to merge balls into K pseudo-domains.

crowd semantics: it projects F into a compact semantic feature and further re-encodes it with a learnable semantic codebook to obtain a refined representation for density map regression. In contrast, the style branch captures domain-related appearance variations and provides regularization signals that facilitate disentanglement and reduce semantic–style information leakage.

To introduce latent domain structure without domain labels, we instantiate Eq. (1) on domain-sensitive feature statistics \mathbf{r}_i , computed from the means and standard deviations of multi-level features. Instead of directly clustering individual samples, we first partition the evolving latent features into compact granular balls, and then cluster granular ball centers as representatives to obtain K pseudo-domains. In this way, direct sample-level flat clustering is transformed into a hierarchical representative-based clustering process, which improves the stability of pseudo-domain assignments during training. Based on the resulting pseudo-domains, we compute domain-wise centers and enforce domain-structured constraints to facilitate robust representation learning. During inference, we discard the style branch and predict density maps using only the semantic branch with codebook re-encoding. In the following, we present the semantic codebook re-encoding, the style-branch regularization, and the granular ball guided stable latent domain discovery module in detail.

A. Semantic Codebook Re-encoding

The semantic branch aims to learn stable counting semantics that are shared across the discovered latent domains. Given the fused feature F , we first project it with a 1×1 convolution to obtain a semantic feature map $S \in \mathbb{R}^{H' \times W' \times d}$. To enhance semantic compactness and improve robustness to domain-specific appearance variations, we introduce a learnable semantic codebook $E = [e_1, \dots, e_{M_c}] \in \mathbb{R}^{d \times M_c}$ and re-encode each spatial location by soft assignment. Let $s_j \in \mathbb{R}^d$ denote the feature vector at spatial location j . We compute the assignment weights as

$$a_j = \text{Softmax}\left(\frac{E^\top s_j}{\sqrt{d}}\right) \in \mathbb{R}^{M_c}, \quad (2)$$

and obtain the re-encoded semantic feature

$$\tilde{s}_j = E a_j \in \mathbb{R}^d. \quad (3)$$

Stacking all $\{\tilde{s}_j\}$ yields the refined semantic feature map \tilde{S} , which is then fed into the density regressor to predict the density map \hat{y} . During inference, we keep only the semantic branch with codebook re-encoding for density estimation.

To further encourage consistency of semantic representations across pseudo-domains, we align image-level semantic descriptors derived from the re-encoded features. For each image, we compute the global semantic descriptor $p_i =$

$\text{GAP}(\tilde{S}_i) \in \mathbb{R}^d$, and denote the batch indices belonging to pseudo-domain k as \mathcal{I}_k . Let

$$\nu_k = \frac{1}{|\mathcal{I}_k|} \sum_{i \in \mathcal{I}_k} p_i, \quad \nu = \frac{1}{B} \sum_{i=1}^B p_i, \quad (4)$$

where ν_k is the semantic center of pseudo-domain k within the mini-batch, and ν is the global batch semantic center. We minimize

$$\mathcal{L}_{\text{sem}} = \frac{1}{|\mathcal{K}_B|} \sum_{k \in \mathcal{K}_B} \|\nu_k - \nu\|_2^2, \quad (5)$$

where $\mathcal{K}_B = \{k \mid |\mathcal{I}_k| > 0\}$. This objective encourages different pseudo-domains to share a more consistent semantic basis, thereby enhancing domain-invariant counting representation learning.

B. Style Branch Regularization

The style branch is designed to model domain-specific appearance variations based on the discovered pseudo-domains. Given the shared multi-scale feature F , we apply a lightweight 1×1 convolutional projection in parallel to the semantic branch, and obtain a style feature map

$$T \in \mathbb{R}^{H' \times W' \times d}. \quad (6)$$

Unlike the semantic branch, T is not used for density estimation. Instead, it provides domain-structured regularization signals that help separate domain-related appearance factors from counting-relevant semantics.

Given the pseudo-domain labels $\{\hat{d}_i\}_{i=1}^B$ obtained by the stable latent domain discovery module, we define the index set of samples assigned to pseudo-domain k as $\mathcal{I}_k = \{i \mid \hat{d}_i = k\}$, and denote the pseudo-domains appearing in the current batch by $\mathcal{K}_B = \{k \mid |\mathcal{I}_k| > 0\}$. We summarize the style feature of each image by global average pooling and compute the corresponding pseudo-domain style center as

$$\begin{aligned} t_i &= \text{GAP}(T_i) \in \mathbb{R}^d, \\ \bar{t}_k &= \frac{1}{|\mathcal{I}_k|} \sum_{i \in \mathcal{I}_k} t_i. \end{aligned} \quad (7)$$

To encourage style consistency within each pseudo-domain, we minimize the intra-domain variance:

$$\mathcal{L}_{\text{sty}} = \frac{1}{|\mathcal{K}_B|} \sum_{k \in \mathcal{K}_B} \frac{1}{|\mathcal{I}_k|} \sum_{i \in \mathcal{I}_k} \|t_i - \bar{t}_k\|_2^2. \quad (8)$$

This objective encourages samples belonging to the same pseudo-domain to share more compact appearance statistics, thereby providing cleaner domain-wise style supervision for disentangled representation learning.

To further reduce information leakage between semantic and style representations, we impose an orthogonality constraint at the spatial level. Let S and T denote the pre-encoded semantic and style feature maps before codebook re-encoding, respectively, and flatten them as $S^{\text{flat}} \in \mathbb{R}^{d \times H'W'}$ and $T^{\text{flat}} \in \mathbb{R}^{d \times H'W'}$. We penalize the squared cosine similarity between the corresponding spatial vectors:

$$\mathcal{L}_{\text{orth}} = \frac{1}{H'W'} \sum_{j=1}^{H'W'} \left(\frac{\tau_j^\top s_j}{\|\tau_j\|_2 \|s_j\|_2 + \epsilon} \right)^2, \quad (9)$$

where s_j and τ_j are the j -th column vectors of S^{flat} and T^{flat} , respectively, and ϵ is a small constant for numerical stability. In implementation, we stop gradients on the semantic feature when computing $\mathcal{L}_{\text{orth}}$, so that this constraint mainly updates the style branch and prevents the semantic branch from being overly disturbed. In this way, the style branch is encouraged to encode domain-related appearance factors that are complementary, rather than redundant, to the semantic counting representation.

C. Granular Ball Guided Stable Latent Domain Discovery

A key challenge in single-source domain generalization is how to stably discover latent domain structure from evolving sample representations. Existing pseudo-domain discovery methods typically perform flat clustering directly on sample-level features, which is vulnerable to noisy samples, outliers, and representation drift during training. To address this issue, we propose a granular ball guided stable latent domain discovery strategy. Instead of clustering all samples directly, we first organize the domain-sensitive descriptors into compact local granular balls, and then cluster granular ball centers as representatives to obtain K pseudo-domains. In this way, direct sample-level clustering is transformed into a hierarchical representative-based clustering process, yielding more stable pseudo-domain assignments under a single labeled source domain. The overall procedure is summarized in Algorithm 1.

At each update stage (e.g., once per epoch), we extract a domain-sensitive descriptor for every source sample. Given a source image x_i , the backbone produces intermediate feature maps $\{F_i^{(l)}\}_{l=1}^L$. We compute channel-wise statistics at each level as

$$\mu_i^{(l)} = \text{Mean}(F_i^{(l)}), \quad \sigma_i^{(l)} = \text{Std}(F_i^{(l)}), \quad (10)$$

and concatenate them into an instance descriptor

$$z_i = [\mu_i^{(1)}, \sigma_i^{(1)}, \dots, \mu_i^{(L)}, \sigma_i^{(L)}] \in \mathbb{R}^D. \quad (11)$$

These statistics are sensitive to appearance and style variations, and are therefore suitable for discovering latent domains. We further apply PCA to obtain a reduced descriptor $\tilde{z}_i \in \mathbb{R}^d$, and denote the reduced descriptor set by

$$\tilde{\mathcal{Z}} = \{\tilde{z}_i\}_{i=1}^N. \quad (12)$$

A granular ball $B \subset \tilde{\mathcal{Z}}$ is defined as a compact subset of descriptors with center

$$c_B = \frac{1}{|B|} \sum_{\tilde{z} \in B} \tilde{z}. \quad (13)$$

To improve splitting flexibility in the reduced feature space, we associate each ball with a non-negative feature-weight vector $w_B \in \mathbb{R}^d$ satisfying $\sum_{j=1}^d w_{B,j} = 1$, and define the weighted distance between a descriptor \tilde{z} and a center c as

$$d_{w_B}(\tilde{z}, c) = \sqrt{\sum_{j=1}^d w_{B,j} (\tilde{z}_j - c_j)^2}. \quad (14)$$

Starting from the root ball containing all descriptors, we recursively split each candidate ball into two child balls via

weighted 2-means. For each split attempt, we initialize the two centroids by farthest-point seeding within the parent ball, perform an initial assignment, and then iterate assignment, centroid update, and weight update until convergence. Given a ball B , we solve

$$\begin{aligned} \min_{\{u_{i\ell}\}, \{\theta_\ell\}, w} & \sum_{\ell=1}^2 \sum_{\tilde{z}_i \in B} \sum_{j=1}^d u_{i\ell} w_j^\beta (\tilde{z}_{i,j} - \theta_{\ell,j})^2, \\ \text{s.t.} & \sum_{\ell=1}^2 u_{i\ell} = 1, \quad u_{i\ell} \in \{0, 1\}, \\ & w_j \geq 0, \quad \sum_{j=1}^d w_j = 1, \end{aligned} \quad (15)$$

where $\theta_\ell \in \mathbb{R}^d$ denotes the ℓ -th centroid and $\beta > 1$ controls the sharpness of the feature weights. We optimize Eq. (15) by alternating updates of assignments $\{u_{i\ell}\}$, centroids $\{\theta_\ell\}$, and weights w . Let

$$D_j = \sum_{\ell=1}^2 \sum_{\tilde{z}_i \in B} u_{i\ell} (\tilde{z}_{i,j} - \theta_{\ell,j})^2 \quad (16)$$

denote the within-cluster scatter on dimension j . The feature weights are updated by inverse-scatter normalization:

$$w_j = \begin{cases} 0, & D_j = 0, \\ \left(\sum_{t=1}^d \left(\frac{D_j + \epsilon}{D_t + \epsilon} \right)^{\frac{1}{\beta-1}} \right)^{-1}, & D_j \neq 0, \end{cases} \quad (17)$$

where ϵ is a small constant. Intuitively, dimensions with smaller within-ball scatter receive larger weights, which leads to more discriminative local partitioning.

Not every split is accepted. We measure the compactness of a ball B by the mean weighted deviation

$$\text{Dm}(B; w_B) = \frac{1}{|B|} \sum_{\tilde{z} \in B} d_{w_B}(\tilde{z}, c_B). \quad (18)$$

Suppose splitting B produces two child balls B_1 and B_2 with a shared weight vector w learned from Eq. (15). Their size-weighted compactness is computed as

$$\text{Dm}_{\text{child}} = \frac{|B_1| \text{Dm}(B_1; w) + |B_2| \text{Dm}(B_2; w)}{|B_1| + |B_2|}. \quad (19)$$

We accept the split if

$$\text{Dm}_{\text{child}} < \tau \text{Dm}(B; w_B), \quad (20)$$

where τ is a fixed split margin. If the condition holds, the parent ball is replaced by its two children and the recursive splitting continues; otherwise, the parent ball is kept as a final ball. We repeat this divide-and-test procedure until no further split is accepted, or a predefined maximum depth is reached, resulting in a final granular ball set

$$\mathcal{B} = \{B_m\}_{m=1}^{M_b}. \quad (21)$$

After hierarchical division, we compute a representative center for each granular ball:

$$g_m = \frac{1}{|B_m|} \sum_{\tilde{z} \in B_m} \tilde{z}. \quad (22)$$

Instead of directly clustering all sample descriptors, we run standard K -means on the granular ball centers $\{g_m\}_{m=1}^{M_b}$ to obtain K pseudo-domains. Each sample then inherits the pseudo-domain label of the granular ball it belongs to. In this way, the final pseudo-domain partition is derived from representative-level clustering rather than sample-level flat clustering. When the number of valid granular balls is insufficient (e.g., $M_b < K$), we directly apply K -means to all descriptors $\tilde{\mathcal{Z}}$ as a fallback.

Since pseudo-domains are re-discovered online, cluster indices may permute across epochs. To maintain label consistency over training, we align the newly obtained pseudo-domain labels with those from the previous epoch using maximum-overlap assignment (Hungarian matching), and reindex the current clusters accordingly. The aligned pseudo-domain labels are then written back to the dataset and used for domain-structured training in the subsequent epoch.

D. Time Complexity of Granular Ball Division

We analyze the time complexity of the hierarchical granular ball division used in our stable latent domain discovery. Let N be the number of descriptors, d the reduced feature dimension, and h_{\max} the maximum division depth. Consider splitting a ball B with $|B| = n$ via weighted 2-means. Each alternating iteration updates assignments, centers, scatters $\{D_j\}$, and feature weights w with cost $\mathcal{O}(nd)$, and computing the compactness in Eq. (18) also requires $\mathcal{O}(nd)$. Therefore, one split attempt costs $\mathcal{O}(Tnd)$ with T alternating iterations.

Across the hierarchy, at a fixed depth the sample sizes of all candidate balls sum to N , so the total cost per depth is $\mathcal{O}(TNd)$. Over at most h_{\max} depths, the overall complexity is bounded by

$$\mathcal{O}(TNd h_{\max}). \quad (23)$$

Since d , T , and h_{\max} are fixed hyper-parameters in our implementation, the resulting division cost scales linearly with the sample size N , i.e., $\mathcal{O}(N)$.

In practice, the split rule in Eq. (20) triggers early stopping for many balls, so the average runtime is often lower than this worst-case upper bound. After hierarchical division, the subsequent K -means is performed on M_b granular ball centers rather than on all N sample descriptors. Because $M_b \ll N$ in practice, this representative-level clustering introduces only a relatively small additional cost compared with direct sample-level clustering.

E. Training Objective and Optimization

We train the network by combining the density regression loss with the proposed domain-structured regularizers:

$$\mathcal{L} = \mathcal{L}_{\text{den}} + \lambda_{\text{sem}} \mathcal{L}_{\text{sem}} + \lambda_{\text{sty}} \mathcal{L}_{\text{sty}} + \lambda_{\text{orth}} \mathcal{L}_{\text{orth}}. \quad (24)$$

We supervise density estimation by a pixel-wise regression loss:

$$\mathcal{L}_{\text{den}} = \frac{1}{B} \sum_{i=1}^B \|\hat{y}_i - y_i\|_2^2, \quad (25)$$

where \hat{y}_i and y_i denote the predicted and ground-truth density maps of the i -th image, respectively. The remaining terms

Algorithm 1 Granular ball guided stable latent domain discovery

Require: Descriptors $\{z_i\}_{i=1}^N$; PCA dimension d ; pseudo-domain number K ; split margin τ ; weight sharpness β ; maximum depth D_{\max} ; ϵ ; (optional) previous labels \hat{d}^{prev} .

Ensure: Pseudo-domain labels $\{\hat{d}_i\}_{i=1}^N$.

- 1: $\tilde{z}_i \leftarrow \text{PCA}(z_i) \in \mathbb{R}^d$ for all i ; initialize the root ball $B_0 = \{\tilde{z}_i\}$ with $w_{B_0} = \frac{1}{d}\mathbf{1}$.
- 2: Initialize queue $\mathcal{Q} \leftarrow \{(B_0, 0)\}$ and leaf set $\mathcal{B} \leftarrow \emptyset$.
- 3: **while** \mathcal{Q} is not empty **do**
- 4: Pop (B, dep) from \mathcal{Q} .
- 5: $(B_1, B_2, w) \leftarrow$ weighted 2-means on B (farthest-point initialization; alternating updates of assignments, centroids, and weights using Eq. (15) and Eq. (17)).
- 6: Compute $\text{Dm}(B_1; w)$, $\text{Dm}(B_2; w)$, and Dm_{child} using Eq. (18).
- 7: **if** $\text{Dm}_{\text{child}} < \tau \text{Dm}(B; w_B)$ **and** $\text{dep} < D_{\max}$ **then**
- 8: Push $(B_1, \text{dep}+1)$ and $(B_2, \text{dep}+1)$ into \mathcal{Q} with $w_{B_1} = w_{B_2} = w$.
- 9: **else**
- 10: $\mathcal{B} \leftarrow \mathcal{B} \cup \{B\}$.
- 11: **end if**
- 12: **end while**
- 13: **if** $|\mathcal{B}| < K$ **then**
- 14: Run K -means on $\{\tilde{z}_i\}_{i=1}^N$ to obtain $\{\hat{d}_i\}$.
- 15: **else**
- 16: Compute granular ball centers g_m for all $B_m \in \mathcal{B}$.
- 17: Run K -means on $\{g_m\}$ to obtain K pseudo-domains.
- 18: Assign each sample the label of the granular ball it belongs to, yielding $\{\hat{d}_i\}$.
- 19: **end if**
- 20: **if** \hat{d}^{prev} is available **then**
- 21: Align current labels to \hat{d}^{prev} by Hungarian matching and reindex $\{\hat{d}_i\}$.
- 22: **end if**
- 23: **return** $\{\hat{d}_i\}_{i=1}^N$.

encourage semantic consistency across the discovered latent domains, intra-domain style compactness, and semantic–style disentanglement, respectively.

Notably, granular ball guided stable latent domain discovery is not introduced as an additional differentiable loss term. Instead, it is performed online to update pseudo-domain labels, which in turn provide the structural supervision required by \mathcal{L}_{sem} and \mathcal{L}_{sty} . In this way, stable latent domain discovery and representation learning are coupled through iterative pseudo-domain refinement during training.

IV. EXPERIMENTS

A. Datasets

We conduct experiments on four widely-used crowd counting benchmarks: ShanghaiTech Part A [1] (SHA), ShanghaiTech [1] Part B (SHB), UCF_QNRF [10] (QNRF), and NWPU-Crowd [11] (NWPU). SHA contains 482 images with diverse resolutions and heavy congestion (501 persons per image on average), while SHB is comparatively sparse with

a resolution of 768×1024 and 123 persons per image on average. QNRF contains 1,535 images with 1,251,642 head annotations, where 1,201 images are used for training and 334 for testing. NWPU is a large-scale dataset comprising 5,109 images annotated with 2.13 million points; it provides 3,109/500/1,500 images for train/val/test splits, respectively, and the test annotations are hidden (evaluation is performed via the official server).

B. Experimental Setting

Following the single-source domain generalization protocol, we train the model on one labeled source dataset and directly evaluate it on the other unseen datasets without any target-domain fine-tuning or adaptation. Head center annotations are converted into density maps by Gaussian convolution with a fixed kernel size of 15. For fair comparison, we adopt the same backbone as DGCC [18], i.e., an encoder-decoder architecture with a 1×1 convolution density estimator. Unless otherwise specified, we train for 200 epochs with 100 iterations per epoch. Input patches are randomly cropped/resized to 320×320 with random horizontal flipping. We use the Adam optimizer with a learning rate of 1×10^{-5} and a weight decay of 1×10^{-4} . All experiments are conducted with batch size 1 on an NVIDIA A100-SXM-64GB GPU. For stable latent domain discovery, we set the number of pseudo-domains K according to the source dataset and update the pseudo-domain labels online every epoch. Specifically, we use $K=4/3/6$ when the source dataset is SHA/SHB/QNRF, respectively. For granular ball division, we use a fixed split margin $\tau=1.05$ in all experiments. We report mean absolute error (MAE) and mean squared error (MSE) of crowd counts.

C. Comparison with State of the Art

Tables I and II summarize the cross-domain comparisons under the single-source, *no-adaptation* protocol (adaptation-based methods are listed separately for reference). Overall, the proposed method demonstrates stable generalization across all source→target transfers. In Table I, it achieves the lowest MAE among no-adaptation methods in every setting while keeping MSE consistently competitive, indicating improved robustness under domain shift. These gains are particularly evident under large domain gaps, where stable latent domain discovery becomes more critical. For example, on the challenging SHB→QNRF transfer, our method improves upon the strongest no-adaptation baseline DGCC [18] from 179.1/316.2 to 165.3/292.0 (MAE/MSE), suggesting fewer large-count outliers and better stability on highly diverse target scenes. Notably, despite using no target-domain data, the proposed method also yields competitive performance relative to adaptation-based approaches, and even surpasses them on the difficult SHB→QNRF transfer.

We further stress-test generalization by using QNRF as the source and transferring to ShanghaiTech. As shown in Table II, the proposed method achieves the best performance on QNRF→SHA with 64.1/103.5 (MAE/MSE), outperforming prior methods by a clear margin. On QNRF→SHB, it remains competitive at 13.0/21.5, achieving a result comparable to

TABLE I

COMPARISON WITH STATE-OF-THE-ART METHODS ON SHA, SHB(MAE/MSE). ADAPT INDICATES WHETHER TEST-TIME TARGET-DOMAIN ADAPTATION IS USED. RESULTS ARE GROUPED BY THE SOURCE TRAINING SET (SHA OR SHB) AND EVALUATED ON THE REMAINING UNSEEN DATASETS. BOLD AND UNDERLINED VALUES DENOTE THE BEST RESULTS WITH ADAPT= \times AND ADAPT= \checkmark , RESPECTIVELY.

Source		SHA				SHB			
Target		SHB		QNRf		SHA		QNRf	
Method	Adapt	MAE	MSE	MAE	MSE	MAE	MSE	MAE	MSE
MCNN [1]	\times	85.2	142.3	–	–	221.4	357.8	–	–
DSSINet [49]	\times	21.7	37.6	198.7	329.4	148.9	273.9	267.3	477.6
BL [6]	\times	15.9	25.8	166.7	287.6	138.1	228.1	226.4	411.0
DMCount [3]	\times	23.1	34.9	134.4	252.1	143.9	239.6	203.0	386.1
D2CNet [50]	\times	21.6	34.6	126.8	245.5	164.5	286.4	267.5	486.0
SASNet [51]	\times	21.3	33.2	211.2	418.6	132.4	225.6	273.5	481.3
MAN [52]	\times	22.1	32.8	138.8	266.3	133.6	255.6	209.4	378.8
DG-MAN [18], [52]	\times	17.3	28.7	129.1	238.2	130.7	225.1	182.4	325.8
DGCC [18]	\times	12.6	24.6	119.4	216.6	121.8	203.1	179.1	316.2
Ours	\times	12.3	21.6	116.2	211.7	117.3	187.1	165.3	292.0
CycleGAN [53]	\checkmark	25.4	39.7	257.3	400.6	143.3	204.3	257.3	400.6
SE CycleGAN [54]	\checkmark	19.9	28.3	230.4	384.5	123.4	193.4	230.4	384.5
SE+FD [55]	\checkmark	16.9	24.7	221.2	390.2	129.3	<u>187.6</u>	221.2	390.2
RBT [56]	\checkmark	13.4	29.3	175.0	294.8	<u>112.2</u>	218.2	211.3	381.9
C ² MoT [57]	\checkmark	12.4	21.1	125.7	218.3	120.7	192.0	198.9	368.0
SaKnD [39]	\checkmark	17.1	27.7	120.2	217.7	137.2	224.2	<u>184.5</u>	<u>320.5</u>
FSIM [58]	\checkmark	<u>11.1</u>	<u>19.3</u>	<u>105.3</u>	<u>191.1</u>	120.3	202.6	194.9	324.5

TABLE II
GENERALIZATION FROM QNRf TO SHANGHAI TECH.

Source	QNRf			
	SHA		SHB	
Target	MAE	MSE	MAE	MSE
DMCount [3]	73.4	135.1	14.3	27.5
SASNet [51]	73.9	116.4	13.0	22.1
MAN [52]	67.1	122.1	12.5	22.2
DGCC [18]	67.4	112.8	12.1	20.9
Ours	64.1	103.5	13.0	21.5

the strongest competitor. These results further verify that the proposed granular ball guided stable latent domain discovery strategy can provide reliable structural supervision and strong transferability under severe cross-dataset shifts.

We additionally evaluate the proposed method on the large-scale NWPU-Crowd benchmark for a more challenging out-of-domain test. As reported in Table III, the proposed method consistently achieves the lowest MSE across all three training settings, indicating improved robustness with fewer extreme errors on diverse scenes and wide count ranges. This trend is particularly meaningful on NWPU, where scenes are highly heterogeneous and the count distribution exhibits a pronounced

long tail, making counting models more prone to catastrophic overestimation or underestimation.

In particular, when trained on SHB, the proposed method improves both metrics over DGCC [18] (MAE 175.0 \rightarrow 173.4, MSE 688.6 \rightarrow 598.5), showing a clear reduction in large-count outliers. We attribute this gain to the proposed granular ball guided stable latent domain discovery strategy, which provides more reliable pseudo-domain assignments and stabilizes domain-wise statistics during training, thereby mitigating spurious style correlations under severe shifts. When trained on SHA or SHA+SHB, the proposed method still delivers clear MSE reductions (e.g., 567.6 \rightarrow 546.2 and 553.6 \rightarrow 545.0), while maintaining comparable MAE. Overall, the consistent MSE improvements across settings suggest that the proposed method not only improves average counting accuracy but also reduces high-variance predictions, leading to more reliable counting under challenging out-of-domain conditions. For the joint-source setting (SHA+SHB), we set the pseudo-domain number to $K=5$.

Fig. 4 presents qualitative comparisons on the unseen QNRf target domain under the no-adaptation setting. For fair comparison, all methods are initialized from the publicly released SHA pre-trained weights provided by their official implementations, and our visualizations are also produced using the SHA pre-trained model without any target-domain fine-tuning. The target scenes exhibit pronounced domain shifts in both appearance and imaging conditions, including large perspective variations, complex illumination, and wide density

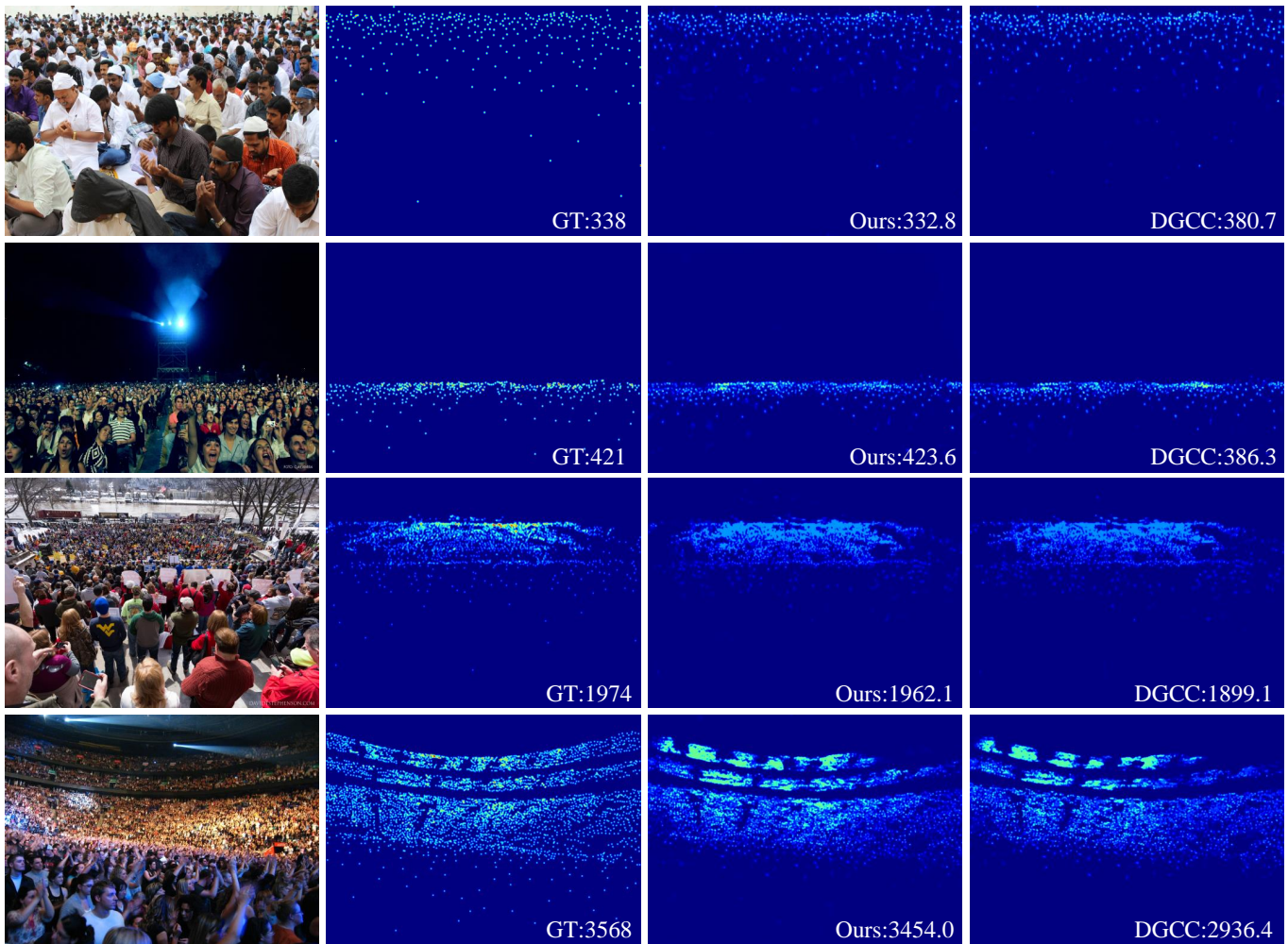


Fig. 4. Qualitative comparison on UCF_QNRF under the *no-adaptation* setting. From left to right: input image, GT density map, and the predictions of Ours, DGCC. The numbers denote crowd counts obtained by integrating the density maps.

TABLE III
ADDITIONAL EVALUATION ON NWPU-CROWD UNDER A NO-ADAPTATION SETTING. MODELS ARE TRAINED ON SHA, SHB, OR THEIR UNION, AND DIRECTLY TESTED ON NWPU.

Source	SHA		SHB		SHA+SHB	
	MAE	MSE	MAE	MSE	MAE	MSE
Target	NWPU					
Method	MAE	MSE	MAE	MSE	MAE	MSE
DMCount [3]	146.9	563.8	191.6	747.4	144.6	592.8
SASNet [51]	158.8	588.0	195.7	716.8	155.3	583.6
MAN [52]	148.2	586.5	193.6	802.5	147.8	605.3
DGCC [18]	143.1	567.6	175.0	688.6	139.6	553.6
Ours	144.3	546.2	173.4	598.5	144.1	545.0

ranges. Under these shifts, the proposed method produces more faithful and spatially structured density maps: responses are more accurately concentrated on true crowd regions, the global crowd layout is better preserved, and density magnitudes remain more coherent across near- and far-field

areas. As a result, the predictions are less affected by over-smoothing and background interference, leading to density distributions that better match the ground-truth structure. We attribute this behavior to the proposed granular ball guided stable latent domain discovery strategy, which provides more reliable structural supervision and helps the model maintain clearer semantic focus under severe cross-domain shifts. In contrast, DGCC [18] tends to suffer from density mass drift under challenging conditions, showing weakened responses in distant congested regions, blurred density patterns, and occasional spurious activations triggered by background textures or illumination changes.

D. Ablation Study

1) *Effect of Stable Latent Domain Discovery*: We study the impact of latent domain discovery, focusing on the discovery strategy rather than the choice of the pseudo-domain number. For a clean module ablation, we fix the number of pseudo-domains and discuss how to select K in the next subsection. Following common practice, we set $K=4$ on SHA, $K=3$ on SHB, and $K=6$ on UCF_QNRF, while keeping the backbone,

TABLE IV

ABLATION ON STABLE LATENT DOMAIN DISCOVERY (MAE/MSE; LOWER IS BETTER). WE FIX K FOR A CLEAN MODULE ABLATION ($K=4$ ON SHA, $K=3$ ON SHB, AND $K=6$ ON UCF_QNRF); THE CHOICE OF K IS DISCUSSED IN THE NEXT SUBSECTION. WE COMPARE RANDOM GROUPING, DIRECT SAMPLE-LEVEL K-MEANS, AND OUR GRANULAR BALL REPRESENTATIVE CLUSTERING STRATEGY. BEST RESULTS ARE HIGHLIGHTED IN BOLDFACE.

Source	SHA				SHB				UCF_QNRF			
	SHB		QNRF		SHA		QNRF		SHA		SHB	
Target	MAE	MSE	MAE	MSE	MAE	MSE	MAE	MSE	MAE	MSE	MAE	MSE
Random grouping	12.8	23.4	119.4	218.4	120.2	210.2	169.2	307.1	68.6	114.6	14.3	27.0
Direct sample-level K-means	12.9	24.4	119.8	219.6	122.7	220.2	166.1	295.3	68.0	111.3	13.5	25.3
Granular ball representative clustering	12.3	21.6	116.2	211.7	117.3	187.1	165.3	292.0	64.1	103.5	13.0	21.5

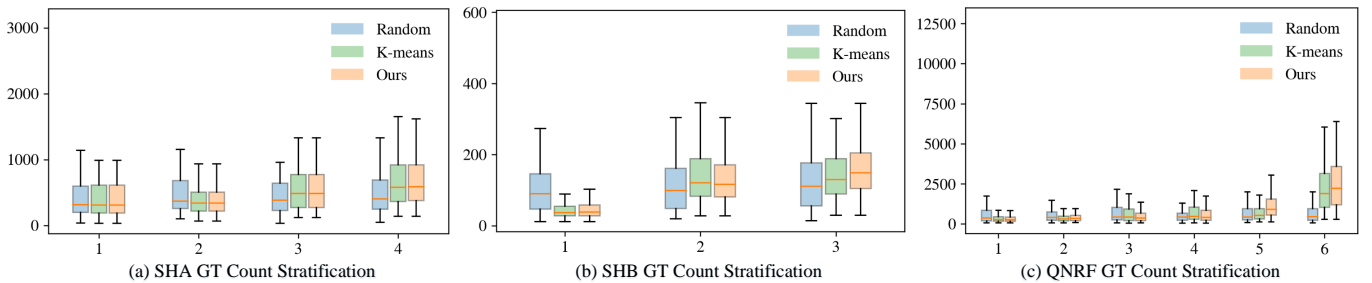


Fig. 5. GT-count stratification across discovered latent domains. Boxplots of GT counts within each pseudo-domain on (a) SHA, (b) SHB, and (c) QNRF. Pseudo-domains are sorted by the median GT count. Compared with Random grouping and direct K-means, the proposed granular ball strategy shows clearer separation with more distinct medians and reduced interquartile overlap, especially on the long-tailed QNRF.

training schedule, and all loss weights unchanged. We only vary how pseudo-domain labels are generated: (i) Random grouping, which uniformly shuffles and splits the training set into K groups as a structure-free sanity check; (ii) Direct sample-level K-means, which follows the clustering baseline used in [18]; and (iii) Granular ball guided representative clustering (ours), which first constructs compact granular balls and then clusters granular ball centers into K pseudo-domains. Table IV summarizes the results.

Under the same fixed K , our latent domain discovery strategy yields the best transfer performance across all six source→target settings, indicating that the way pseudo-domains are constructed remains crucial even when the number of groups is held constant. Compared with Random grouping, our method brings consistent improvements, with a clear gain on the challenging QNRF→SHA transfer (64.1/103.5 vs. 68.6/114.6). Compared with direct sample-level K-means [18], our method also improves all settings and shows larger benefits under larger domain gaps. Although Random grouping can be competitive in a few cases, its behavior is inconsistent, suggesting that the improvements do not come from arbitrary grouping, but from a more stable and structure-aware latent domain discovery process.

Beyond transfer accuracy, we further investigate whether the discovered pseudo-domains align with a meaningful semantic factor in crowd counting, namely the count (density) regime. This perspective also helps explain why a better-separated partition improves transferability: different density regimes induce distinct occlusion patterns, texture statistics, and appearance distributions, and pseudo-domain learning is more effective when each group is internally coherent rather

than mixing sparse and highly crowded samples. A random split tends to average out regime-specific statistics, weakening the pseudo-domain signal, whereas a structure-aware partition yields more homogeneous groups and thus more informative domain-structured regularization, consistent with the gains in Table IV. Using the same fixed K as in Table IV, we summarize each pseudo-domain d by the median ground-truth count m_d . We then quantify how well the partition separates density regimes by measuring the spread of these K medians: $\Delta_{\text{med}} = \max(m_d) - \min(m_d)$ and the standard deviation σ_{med} across $\{m_d\}_{d=1}^K$ (Table V; larger is better). If the partition is close to random, each group mirrors the global count distribution, so the medians remain similar and both Δ_{med} and σ_{med} stay small. Larger values indicate that pseudo-domains are more clearly organized along the density axis, with less mixing between sparse and crowded samples.

Table V shows that Random grouping yields consistently weak separation, while direct sample-level K-means already enlarges the median spread. Our granular ball based method further increases both Δ_{med} and σ_{med} on all datasets. The effect is most prominent on the long-tailed QNRF, where Δ_{med} increases from 1624.7 to 1949.6 and σ_{med} increases from 563.3 to 686.6, indicating clearer isolation of extreme-density regimes. Fig. 5 visualizes the same trend by plotting ground-truth count distributions within each pseudo-domain (sorted by m_d): compared with Random grouping and direct sample-level K-means, our method exhibits more separated medians and reduced interquartile overlap, implying lower intra-domain mixing and clearer regime separation. Together with the transfer improvements in Table IV, these results suggest that the discovered pseudo-domains are not arbitrary

TABLE V

GT-COUNT STRATIFICATION OF DISCOVERED LATENT DOMAINS. FOR EACH METHOD, WE COMPUTE THE MEDIAN GT COUNT m_d FOR EACH PSEUDO-DOMAIN AND REPORT THE RANGE $\Delta_{\text{med}} = \max(m_d) - \min(m_d)$ AND THE STANDARD DEVIATION σ_{med} ACROSS THE K MEDIANS. LARGER VALUES INDICATE CLEARER DENSITY-REGIME SEPARATION.

Dataset	Method	$\Delta_{\text{med}} \uparrow$	$\sigma_{\text{med}} \uparrow$
SHA	Random grouping	90.8	33.8
	Direct K-means	270.9	110.2
	Granular ball	278.0	112.7
SHB	Random grouping	20.7	8.5
	Direct K-means	92.9	41.8
	Granular ball	110.2	46.3
QNRF	Random grouping	72.4	23.5
	Direct K-means	1624.7	563.3
	Granular ball	1949.6	686.6

clusters, but capture semantically meaningful and more stable density-regime structure, thereby providing a more informative supervisory signal for domain-general crowd counting.

2) *Effect of the Number of Latent Domains K* : We study how the number of pseudo-domains K affects stable latent domain discovery and downstream transfer performance. Tables VI and VII report the results on three source datasets with several nearby choices of K . Overall, the performance follows a typical under-/over-partitioning pattern. When K is too small, heterogeneous samples are forced into the same latent domain, which weakens domain-structured regularization due to large intra-domain variance. When K is overly large, the training set is fragmented into many small and noisy groups, making intra-domain and inter-domain statistics less reliable. As a result, intermediate values of K generally provide the best trade-off and yield the lowest MAE/MSE.

For SHA and SHB, the results in Table VI show that the best performance is achieved at $K=4$ and $K=3$, respectively. When the source is SHA, setting $K=4$ yields the lowest MAE/MSE on both SHB and QNRF, while $K=3$ or $K=5$ leads to slightly worse transfer results. When the source is SHB, the optimal choice shifts to a smaller value, i.e., $K=3$, which suggests that the source distribution of SHB is relatively more concentrated and that fewer pseudo-domains provide more stable group statistics for domain-structured regularization. For QNRF, Table VII shows that $K=6$ gives the best performance on both SHA and SHB, outperforming its neighboring choices $K=5$ and $K=7$. This observation is consistent with the larger scale and stronger long-tailed distribution of QNRF: a moderately larger number of latent domains is beneficial for capturing its richer source-domain heterogeneity, while excessive partitioning still harms the reliability of domain-wise statistics.

To avoid tuning K over a wide range when transferring to a new source dataset, we use a simple data-dependent rule to determine a reasonable scale. Given the number of training images N , we compute

$$K_0 = N^{\frac{1}{4}}, \quad (26)$$

TABLE VI

EFFECT OF THE NUMBER OF LATENT DOMAINS K UNDER THE SINGLE-SOURCE DOMAIN-GENERAL SETTING (SOURCE: SHA/SHB).

Source	SHA				SHB			
	Target	SHB		QNRF		SHA		QNRF
K	MAE	MSE	MAE	MSE	MAE	MSE	MAE	MSE
3	12.8	24.3	120.9	218.1	117.3	187.1	165.3	292.0
4	12.3	21.6	116.2	211.7	119.3	202.9	172.7	306.4
5	12.6	23.7	118.3	215.6	117.4	200.7	177.6	322.0

TABLE VII

EFFECT OF THE NUMBER OF LATENT DOMAINS K UNDER THE SINGLE-SOURCE DOMAIN-GENERAL SETTING (SOURCE: QNRF).

Source	QNRF			
	Target	SHA		SHB
K	MAE	MSE	MAE	MSE
5	67.6	109.4	14.0	25.8
6	64.1	103.5	13.0	21.5
7	70.8	113.3	14.3	27.0

and evaluate a few candidates in a small neighborhood around K_0 . This choice grows sublinearly with N , balancing latent domain granularity and the sample size within each group. In our experiments, the best-performing K values are consistently found near the scale suggested by Eq. (26): we use $K=4$ for SHA, $K=3$ for SHB, and $K=6$ for QNRF, as shown in Tables VI and VII. Overall, rather than treating K as a purely empirical hyper-parameter, Eq. (26) offers a transparent guideline that narrows the search to a small range, thereby reducing tuning cost when applying the proposed framework to new source datasets.

3) *Effect of Core Components*: We evaluate the contribution of our two core components: Semantic Codebook Re-encoding (SCR) and Structured Branch Regularization (SBR). All experiments follow the standard single-source domain-general setting: we train on a single source dataset and directly test on unseen target datasets, without any target-domain adaptation. Table VIII reports MAE/MSE over six transfer settings. Starting from the baseline, adding SCR yields consistent improvements across all transfers, suggesting that codebook-based re-encoding helps learn more stable and transferable semantic representations under domain shift. For example, SCR reduces MAE from 134.5 to 123.8 on SHA→QNRF and also improves QNRF→SHB from 18.8/35.6 to 15.4/28.7 (MAE/MSE). Building upon SCR, introducing SBR further strengthens cross-domain generalization and achieves the best overall performance across the transfer settings, including the challenging QNRF→SHA case (69.9→64.1). These results indicate that, beyond improving semantic representation quality, leveraging the discovered latent domains for structured regularization provides additional gains in out-of-domain robustness.

We further analyze the three regularizers in SBR by removing them one at a time. As shown in Table VIII, removing

TABLE VIII
 ABLATION ON THE CORE COMPONENTS, INCLUDING SEMANTIC CODEBOOK RE-ENCODING (SCR) AND STRUCTURED BRANCH REGULARIZATION (SBR) BUILT UPON THE DISCOVERED LATENT DOMAINS, AS WELL AS THE INDIVIDUAL REGULARIZERS IN SBR, UNDER THE SINGLE-SOURCE DOMAIN-GENERAL SETTING (NO TARGET-DOMAIN ADAPTATION).

Source	SHA				SHB				QNRf			
Target	SHB		QNRf		SHA		QNRf		SHA		SHB	
Method	MAE	MSE	MAE	MSE	MAE	MSE	MAE	MSE	MAE	MSE	MAE	MSE
Baseline	14.8	27.7	134.5	230.5	132.6	229.7	190.6	305.9	88.2	145.0	18.8	35.6
+ SCR	13.8	27.2	123.8	228.6	121.7	203.2	171.4	298.9	69.9	116.7	15.4	28.7
+ SBR (Full)	12.3	21.6	116.2	211.7	117.3	187.1	165.3	292.0	64.1	103.5	13.0	21.5
w/o \mathcal{L}_{sem}	13.9	27.0	117.8	214.1	119.3	214.8	172.7	306.4	67.2	111.0	14.1	26.5
w/o \mathcal{L}_{sty}	13.0	24.1	123.0	232.9	122.1	223.6	169.2	307.1	66.5	104.1	14.6	28.8
w/o $\mathcal{L}_{\text{orth}}$	12.7	25.7	125.1	234.5	118.5	209.8	178.7	313.6	71.6	118.6	13.8	25.6

any of \mathcal{L}_{sem} , \mathcal{L}_{sty} , or $\mathcal{L}_{\text{orth}}$ consistently degrades performance, indicating that they contribute complementary effects. In particular, \mathcal{L}_{sem} encourages semantic consistency across the discovered latent domains, \mathcal{L}_{sty} enforces style compactness within each pseudo-domain, and $\mathcal{L}_{\text{orth}}$ promotes semantic–style disentanglement by suppressing feature leakage between the two branches. Overall, SCR strengthens the semantic representation basis, while SBR further improves generalization by exploiting stable latent domain structure to jointly promote semantic consistency, style compactness, and semantic–style disentanglement.

V. CONCLUSION

In this paper, we investigated stable latent domain discovery for single-source domain-general crowd counting. We argued that a key challenge of this problem lies in reliably uncovering latent domain structure from evolving sample representations, where direct sample-level flat clustering is often sensitive to noisy features, outliers, and representation drift. To address this issue, we proposed a granular ball guided stable latent domain discovery framework that first organizes samples into compact local granular balls and then clusters granular ball centers as representatives, thereby transforming direct sample-level clustering into a hierarchical representative-based clustering process. Built upon the discovered latent domains, we further developed a two-branch learning framework, where Semantic Codebook Re-encoding (SCR) enhances stable counting semantics and Structured Branch Regularization (SBR) promotes semantic consistency, style compactness, and semantic–style disentanglement. Extensive experiments on standard DG crowd counting benchmarks, including SHA, SHB, UCF_QNRf, and NWPU-Crowd, demonstrated that the proposed method achieves consistently strong generalization across multiple unseen transfers, with particularly clear gains under large domain gaps.

In future work, we plan to extend the proposed structural modeling strategy to more challenging settings, such as multi-source domain generalization and continuously evolving de-

ployment domains. It is also promising to explore tighter integration with stronger backbones, such as transformer-based encoders, and to investigate more fine-grained structural cues beyond global feature statistics, for example region-aware or density-aware descriptors, to further improve robustness under extreme congestion and complex imaging conditions.

REFERENCES

- [1] Y. Zhang, D. Zhou, S. Chen, S. Gao, and Y. Ma, “Single-image crowd counting via multi-column convolutional neural network,” in *Proceedings of the IEEE conference on computer vision and pattern recognition*, 2016, pp. 589–597.
- [2] Y. Li, X. Zhang, and D. Chen, “Csrnet: Dilated convolutional neural networks for understanding the highly congested scenes,” in *Proceedings of the IEEE conference on computer vision and pattern recognition*, 2018, pp. 1091–1100.
- [3] B. Wang, H. Liu, D. Samaras, and M. H. Nguyen, “Distribution matching for crowd counting,” *Advances in neural information processing systems*, vol. 33, pp. 1595–1607, 2020.
- [4] X. Cao, Z. Wang, Y. Zhao, and F. Su, “Scale aggregation network for accurate and efficient crowd counting,” in *Proceedings of the European conference on computer vision (ECCV)*, 2018, pp. 734–750.
- [5] W. Liu, M. Salzmann, and P. Fua, “Context-aware crowd counting,” in *Proceedings of the IEEE/CVF conference on computer vision and pattern recognition*, 2019, pp. 5099–5108.
- [6] Z. Ma, X. Wei, X. Hong, and Y. Gong, “Bayesian loss for crowd count estimation with point supervision,” in *Proceedings of the IEEE/CVF international conference on computer vision*, 2019, pp. 6142–6151.
- [7] J. Yi, F. Chen, Z. Shen, Y. Xiang, S. Xiao, and W. Zhou, “An effective lightweight crowd counting method based on an encoder–decoder network for internet of video things,” *IEEE Internet of Things Journal*, vol. 11, no. 2, pp. 3082–3094, 2023.
- [8] Z. Shen, G. Li, R. Xia, H. Meng, and Z. Huang, “A lightweight object counting network based on density map knowledge distillation,” *IEEE Transactions on Circuits and Systems for Video Technology*, vol. 35, no. 2, pp. 1492–1505, 2025.
- [9] J. Wang, C. Lan, C. Liu, Y. Ouyang, T. Qin, W. Lu, Y. Chen, W. Zeng, and P. S. Yu, “Generalizing to unseen domains: A survey on domain generalization,” *IEEE transactions on knowledge and data engineering*, vol. 35, no. 8, pp. 8052–8072, 2022.
- [10] H. Idrees, M. Tayyab, K. Athrey, D. Zhang, S. Al-Maadeed, N. Rajpoot, and M. Shah, “Composition loss for counting, density map estimation and localization in dense crowds,” in *Proceedings of the European conference on computer vision (ECCV)*, 2018, pp. 532–546.
- [11] Q. Wang, J. Gao, W. Lin, and X. Li, “Nwpu-crowd: A large-scale benchmark for crowd counting and localization,” *IEEE transactions on pattern analysis and machine intelligence*, vol. 43, no. 6, pp. 2141–2149, 2020.

- [12] J. Gao, T. Han, Y. Yuan, and Q. Wang, "Domain-adaptive crowd counting via high-quality image translation and density reconstruction," *IEEE transactions on neural networks and learning systems*, vol. 34, no. 8, pp. 4803–4815, 2021.
- [13] M. K. K. Reddy, M. Rochan, Y. Lu, and Y. Wang, "Adacrowd: Unlabeled scene adaptation for crowd counting," *IEEE Transactions on Multimedia*, vol. 24, pp. 1008–1019, 2021.
- [14] Y. Ganin, E. Ustinova, H. Ajakan, P. Germain, H. Larochelle, F. Laviolette, M. March, and V. Lempitsky, "Domain-adversarial training of neural networks," *Journal of machine learning research*, vol. 17, no. 59, pp. 1–35, 2016.
- [15] B. Sun and K. Saenko, "Deep coral: Correlation alignment for deep domain adaptation," in *European conference on computer vision*. Springer, 2016, pp. 443–450.
- [16] I. Gulrajani and D. Lopez-Paz, "In search of lost domain generalization," *arXiv preprint arXiv:2007.01434*, 2020.
- [17] K. Zhou, Y. Yang, Y. Qiao, and T. Xiang, "Domain generalization with mixstyle," *arXiv preprint arXiv:2104.02008*, 2021.
- [18] Z. Du, J. Deng, and M. Shi, "Domain-general crowd counting in unseen scenarios," in *Proceedings of the AAAI conference on artificial intelligence*, vol. 37, no. 1, 2023, pp. 561–570.
- [19] G. Ding, L. Liu, Z. Chen, and C. Chen, "Domain-agnostic crowd counting via uncertainty-guided style diversity augmentation," in *Proceedings of the 32nd ACM International Conference on Multimedia*, 2024, pp. 1642–1651.
- [20] Y. Gal and Z. Ghahramani, "Dropout as a bayesian approximation: Representing model uncertainty in deep learning," in *international conference on machine learning*. PMLR, 2016, pp. 1050–1059.
- [21] A. Kendall and Y. Gal, "What uncertainties do we need in bayesian deep learning for computer vision?" *Advances in neural information processing systems*, vol. 30, 2017.
- [22] B. Lakshminarayanan, A. Pritzel, and C. Blundell, "Simple and scalable predictive uncertainty estimation using deep ensembles," *Advances in neural information processing systems*, vol. 30, 2017.
- [23] G. Wang, "Dgcc: data-driven granular cognitive computing," *Granular Computing*, vol. 2, no. 4, pp. 343–355, 2017.
- [24] S. Xia, G. Wang, and X. Gao, "Granular-ball computing: an efficient, robust, and interpretable adaptive multi-granularity representation and computation method," *ArXiv*, vol. abs/2304.11171, 2023. [Online]. Available: <https://api.semanticscholar.org/CorpusID:258298571>
- [25] Q. Xie, Q. Zhang, S. Xia, F. Zhao, C. Wu, G. Wang, and W. Ding, "Gbg++: A fast and stable granular ball generation method for classification," *IEEE Transactions on Emerging Topics in Computational Intelligence*, 2024.
- [26] J. Xie, C. Hua, S. Xia, Y. Cheng, G. Wang, and X. Gao, "W-gbc: An adaptive weighted clustering method based on granular-ball structure," in *2024 IEEE 40th International Conference on Data Engineering (ICDE)*. IEEE, 2024, pp. 914–925.
- [27] D. Cheng, C. Zhang, Y. Li, S. Xia, G. Wang, J. Huang, S. Zhang, and J. Xie, "Gb-dbscan: a fast granular-ball based dbscan clustering algorithm," *Information Sciences*, vol. 674, p. 120731, 2024.
- [28] A. Quadir and M. Tanveer, "Granular ball twin support vector machine with pinball loss function," *IEEE Transactions on Computational Social Systems*, 2024.
- [29] D. Dai, F. Chen, S. Xia, L. Yang, G. Wang, G. Wang, and X. Gao, "An adaptive multi-granularity graph representation of image via granular-ball computing," *IEEE Transactions on Image Processing*, vol. 34, pp. 2986–2999, 2025.
- [30] H. Mo, X. Zhang, J. Tan, C. Yang, Q. Gu, B. Hang, and W. Ren, "Countformer: Multi-view crowd counting transformer," in *European Conference on Computer Vision*. Springer, 2024, pp. 20–40.
- [31] Y. Chen, Q. Wang, J. Yang, B. Chen, H. Xiong, and S. Du, "Learning discriminative features for crowd counting," *IEEE Transactions on Image Processing*, vol. 33, pp. 3749–3764, 2024.
- [32] W. Shu, J. Wan, and A. B. Chan, "Generalized characteristic function loss for crowd analysis in the frequency domain," *IEEE Transactions on Pattern Analysis and Machine Intelligence*, vol. 46, no. 5, pp. 2882–2899, 2023.
- [33] M. Yang, Z. Li, J. Zhang, L. Qi, and Y. Shi, "Taste more, taste better: Diverse data and strong model boost semi-supervised crowd counting," in *Proceedings of the Computer Vision and Pattern Recognition Conference*, 2025, pp. 24 440–24 451.
- [34] H. Lin, Z. Ma, R. Ji, Y. Wang, Z. Su, X. Hong, and D. Meng, "Semi-supervised counting via pixel-by-pixel density distribution modelling," *IEEE Transactions on Pattern Analysis and Machine Intelligence*, 2025.
- [35] H. Meng, X. Hong, C. Wang, M. Shang, and W. Zuo, "Multi-modal crowd counting via a broker modality," in *European Conference on Computer Vision*. Springer, 2024, pp. 231–250.
- [36] H. Meng, X. Hong, Z. Lai, and M. Shang, "Free lunch enhancements for multi-modal crowd counting," in *Proceedings of the Computer Vision and Pattern Recognition Conference*, 2025, pp. 14 013–14 023.
- [37] Y. Ranasinghe, N. G. Nair, W. G. C. Bandara, and V. M. Patel, "Crowddiff: Multi-hypothesis crowd density estimation using diffusion models," in *Proceedings of the IEEE/CVF Conference on Computer Vision and Pattern Recognition*, 2024, pp. 12 809–12 819.
- [38] H. Zhu, J. Yuan, X. Zhong, Z. Yang, Z. Wang, and S. He, "Daot: Domain-agnostically aligned optimal transport for domain-adaptive crowd counting," in *Proceedings of the 31st ACM International Conference on Multimedia*, 2023, pp. 4319–4329.
- [39] H. Xie, Z. Yang, H. Zhu, and Z. Wang, "Striking a balance: Unsupervised cross-domain crowd counting via knowledge diffusion," in *Proceedings of the 31st ACM international conference on multimedia*, 2023, pp. 6520–6529.
- [40] L. Chen, Y. Zhang, Y. Song, Z. Shen, and L. Liu, "Lfme: A simple framework for learning from multiple experts in domain generalization," *Advances in Neural Information Processing Systems*, vol. 37, pp. 102 919–102 947, 2024.
- [41] K. Le, L. Ho, C. Do, D. Le-Phuoc, and K.-S. Wong, "Efficiently assemble normalization layers and regularization for federated domain generalization," in *Proceedings of the IEEE/CVF conference on computer vision and pattern recognition*, 2024, pp. 6027–6036.
- [42] Z. Peng and S.-H. G. Chan, "Single domain generalization for crowd counting," in *Proceedings of the IEEE/CVF Conference on Computer Vision and Pattern Recognition*, 2024, pp. 28 025–28 034.
- [43] L. Chen, "Topological structure in visual perception," *Science*, vol. 218, no. 4573, pp. 699–700, 1982.
- [44] S. Xia, X. Dai, G. Wang, X. Gao, and E. Giem, "An efficient and adaptive granular-ball generation method in classification problem," *IEEE Transactions on Neural Networks and Learning Systems*, vol. 35, no. 4, pp. 5319–5331, 2022.
- [45] S. Xia, D. Peng, D. Meng, C. Zhang, G. Wang, E. Giem, W. Wei, and Z. Chen, "Ball k k-means: Fast adaptive clustering with no bounds," *IEEE transactions on pattern analysis and machine intelligence*, vol. 44, no. 1, pp. 87–99, 2020.
- [46] J. Xie, X. Xiang, S. Xia, L. Jiang, G. Wang, and X. Gao, "Mgnr: A multi-granularity neighbor relationship and its application in knn classification and clustering methods," *IEEE Transactions on Pattern Analysis and Machine Intelligence*, 2024.
- [47] J. Liu, H. Jianye, Y. Ma, and S. Xia, "Unlock the cognitive generalization of deep reinforcement learning via granular ball representation," in *Forty-first International Conference on Machine Learning*, 2024.
- [48] S. Xia, X. Ma, Z. Liu, C. Liu, S. Zhao, and G. Wang, "Graph coarsening via supervised granular-ball for scalable graph neural network training," in *Proceedings of the AAAI Conference on Artificial Intelligence*, vol. 39, no. 12, 2025, pp. 12 872–12 880.
- [49] L. Liu, Z. Qiu, G. Li, S. Liu, W. Ouyang, and L. Lin, "Crowd counting with deep structured scale integration network," in *Proceedings of the IEEE/CVF international conference on computer vision*, 2019, pp. 1774–1783.
- [50] J. Cheng, H. Xiong, Z. Cao, and H. Lu, "Decoupled two-stage crowd counting and beyond," *IEEE Transactions on Image Processing*, vol. 30, pp. 2862–2875, 2021.
- [51] Q. Song, C. Wang, Y. Wang, Y. Tai, C. Wang, J. Li, J. Wu, and J. Ma, "To choose or to fuse? scale selection for crowd counting," in *Proceedings of the AAAI conference on artificial intelligence*, vol. 35, no. 3, 2021, pp. 2576–2583.
- [52] H. Lin, Z. Ma, R. Ji, Y. Wang, and X. Hong, "Boosting crowd counting via multifaceted attention," in *Proceedings of the IEEE/CVF conference on computer vision and pattern recognition*, 2022, pp. 19 628–19 637.
- [53] J.-Y. Zhu, T. Park, P. Isola, and A. A. Efros, "Unpaired image-to-image translation using cycle-consistent adversarial networks," in *Proceedings of the IEEE international conference on computer vision*, 2017, pp. 2223–2232.
- [54] Q. Wang, J. Gao, W. Lin, and Y. Yuan, "Learning from synthetic data for crowd counting in the wild," in *Proceedings of the IEEE/CVF conference on computer vision and pattern recognition*, 2019, pp. 8198–8207.
- [55] T. Han, J. Gao, Y. Yuan, and Q. Wang, "Focus on semantic consistency for cross-domain crowd understanding," in *ICASSP 2020-2020 IEEE International Conference on Acoustics, Speech and Signal Processing (ICASSP)*. IEEE, 2020, pp. 1848–1852.
- [56] Y. Liu, Z. Wang, M. Shi, S. Satoh, Q. Zhao, and H. Yang, "Towards unsupervised crowd counting via regression-detection bi-knowledge

- transfer,” in *Proceedings of the 28th ACM international conference on multimedia*, 2020, pp. 129–137.
- [57] Q. Wu, J. Wan, and A. B. Chan, “Dynamic momentum adaptation for zero-shot cross-domain crowd counting,” in *Proceedings of the 29th ACM International Conference on Multimedia*, 2021, pp. 658–666.
- [58] H. Zhu, J. Yuan, X. Zhong, L. Liao, and Z. Wang, “Find gold in sand: Fine-grained similarity mining for domain-adaptive crowd counting,” *IEEE Transactions on Multimedia*, vol. 26, pp. 3842–3855, 2023.